Biophysical Chemistry, 45 (1993) 201–217
Elsevier Science Publishers B.V., Amsterdam

BIOCHE 01710

Dielectric behavior of polyelectrolytes VII. Dielectric relaxation and Kerr effect of cylindrical biopolymers

Wayne E. Sonnen, Gary E. Wesenberg and Worth E. Vaughan
Department of Chemistry, University of Wisconsin–Madison, Madison, WI 53706 (USA)

(Received 21 May 1992; accepted in revised form 3 August 1992)

Abstract

A model forced diffusion equation is solved for the orientation of cylindrical biopolymers including the configuration of the counterions. The result is used to predict the dielectric relaxation and dynamical Kerr effect of a DNA oligomer for which experimental data appear in the literature. The significant advance in the formalism is the elimination of the counterion condensation assumption. A result is an improved fit of the model prediction to the experimental data. However, discrepancies persist at short times.

Keywords: Polyelectrolytes; Dielectric relaxation; Kerr effect; DNA oligomer; Counterion interaction

1. Introduction

The motion of charged species near the surface of natural polyelectrolytes is an integral part of the dynamic biological function of the polymer. An example is the regulation of gene expression of DNA. This motion can be probed via interaction of the charges of the biopolymer assembly with external electric fields. The linear and quadratic responses determine the dielectric relaxation and Kerr effect, respectively.

A microscopic model formalism for the dynamical response in cylindrical geometry was set forth previously in paper VI [1] of this series. Statistical mechanics was used to relate the microscopic picture to the macroscopic observables. The model adopted the counterion condensation viewpoint in which one presumes that a (known) fraction of the counterions are constrained by electrostatic forces to the surface of the polyelectrolyte. The model thereby acquires a dynamical parameter, the "surface diffusion constant" of a counterion, that is determined by fitting the observed experimental data to the model prediction. Two other parameters should be incorporated. They describe the rate at which condensed counterions exchange with the remaining counterions in the "bulk phase". These parameters enter via the boundary conditions at the surface–bulk interface and are difficult to introduce in a physically appealing manner [2] (paper I of this series). An additional reason for fealing uneasy with the formalism

Correspondence to: W.E. Sonnen, Department of Chemistry, University of Wisconsin–Madison, Madison, WI 53706 (USA).

is that the experimentally observed dynamic Kerr effect for DNA exhibits a spread out response in time, whereas the model prediction is a dominant single exponential mode that leads to a relatively narrow response in time (see in particular the reversing electric field data shown in Fig. 3 of ref. [12]). The difference appears to be attributable to the condensation picture. In this work the surface constraint is eliminated. All counterions are treated equivalently and they are allowed to move in a (large) cylindrical annulus (cell model) [13] with a length corresponding to that of the polyelectrolyte rod and an inner surface corresponding to the surface of the rod. A consequence of this step is that the surface diffusion constant vanishes from the formalism. The fixed charges on the biopolymer play an intimate role in determining the dynamical behavior instead of just being a cause for drawing counterions to the rod surface. The surface–bulk phase boundary is eliminated and the only dynamical parameters of the model are the bulk diffusion coefficient of a counterion and the components of the rotational diffusion tensor of the rod. The bottom line is that allowing motion of the counterions in the radial direction leads to significant dipole moment components in the r- as well as z-direction of the cylinder geometry and produces additional modes supressed previously by the surface constraint.

2. The joint conditional probability density

To compute any time dependent system property in the configuration space of the rod and counterions, we need the joint conditional probability density, P, of finding a molecule (with cylindrical symmetry) with orientation (Euler angles) θ, ϕ and counterion co-ordinates $\{r_i\}$, $\{z_i\}$, $\{\phi_i\}$ given the initial state θ', ϕ', $\{r_i'\}$, $\{z_i'\}$, $\{\phi_i'\}$. With the model picture of rotational diffusion of the molecule and (forced) diffusion of the counterions we write

$$\frac{\partial P}{\partial t} = \nabla_u \cdot \mathbf{D}_R \cdot \nabla_u P + D_3 \sum_i \nabla_i^2 P + \frac{1}{k_B T} \nabla_u \cdot \mathbf{D}_R \cdot P \nabla_u V + \frac{D_3}{k_B T} \sum_i \nabla_i \cdot P \nabla_i V \tag{1}$$

In eq. (1) the first term on the right-hand side describes the anisotropic rotational diffusion of the rod. $\mathbf{D}_R$ is the (diagonal) rotation diffusion tensor with components $D_\perp \hat{x}\hat{x}$, $D_\perp \hat{y}\hat{y}$ and $D_\parallel \hat{z}\hat{z}$ in the molecule fixed co-ordinate system. $D_\perp$ describes diffusion involving motion of the symmetry axis and $D_\perp$ motion around the symmetry axis. ∇_u is the rotation operator [3] ∇_i is the gradient operator [4]. Explicit expressions for the terms in eq. (1) in the configuration space variable set are shown in the Appendix.

The second term describes the free diffusion (diffusion constant D_3) of the counterions in bulk. The co-ordinate system describing the counterion diffusion is in a molecule fixed basis. We treat the polyion–counterion assembly as an extended molecule that diffuses (in θ, ϕ) as a whole. The alternative extreme that presumes only the cylindrical core undergoes rotational diffusion seems unphysical. Although the counterions are not covalently bound to the core, they feel the strong electrostatic attraction of the phosphate charges and tend to be imbedded in the first few layers of hydration. Diffusion of the counterions is pictured as a "jump and hold" mechanism where a (hydrated) counterion exchanges its coordinate with a solvent cluster. In effect we have ignored a potential coupling between the first two terms in eq. (1). This ansatz is a point of controversy and results from use of the primitive model. The solvent structure that stabilizes certain counterion configurations is not part of the microscopic picture. Hydrodynamic effects are also not treated. This is the price we pay for attempting a molecular as opposed to phenomenological formalism. Fortunately, the rotational diffusion of the cylinder does not contribute much to the relaxation rates that arise in the model calculation; the results would be similar if we assumed that the cylinder did not diffuse at all; in this case the question of molecule fixed versus space fixed co-ordinate systems for the surroundings would be moot. We

emphasize that the extended molecule picture only applies to the first few hydration layers. However, virtually all the counterions are found in this region.

The third term in eq. (1) deals with the role of an applied electric field in modifying the motion of the rod in space.

The potential V is the interaction with the external field E plus the Coulomb repulsions of the counterions (V') and the interactions of the counterions with fixed charges on the rod (V'').

$$V = -E\cos\theta\mu_z - E\sin\theta\sin\phi\mu_x - E\sin\theta\cos\phi\mu_y + V' + V'' \tag{2}$$

$$V' = \sum_{ij}{}' \frac{e^2}{4\pi\varepsilon\varepsilon_0 |r_i - r_j|} \tag{3}$$

The double sum in V' is over pairwise counterion interactions and is the Coulombic repulsion of the set of counterions in a continuous solvent of relative dielectric constant ε. The expression for V'' is similar (opposite sign) except it involves only a single sum over counterion positions.

The dipole moment components are (L is the rod length and e the magnitude of the electron charge)

$$\mu_x = e\sum_i r_i\cos\phi_i, \qquad \mu_y = e\sum_i r_i\sin\phi_i, \qquad \mu_z = e\sum_i (z_i - L/2) \tag{4}$$

The final term in eq. (1) represents the role of the potential in modifying the motion of the counterions.

Equation (1) is solved for P via a high-temperature expansion (powers of E/k_BT). For boundary conditions we choose (alternatives were considered in paper IV of this series [5]): $P(\phi) = P(\phi + 2\pi)$; $P(\phi_i) = P(\phi_i + 2\pi)$; $\partial P/\partial r_i = 0$; $r_i = r_1$ or r_2 (r_1 and r_2 are the boundaries of a cell in which the counterions move); $\partial P/\mathrm{d}z_i = 0$, $z_i = 0$ or L (no flux of probability density at the ends of the cylindrical annulus comprising the cell).

P can be expanded in a complete set of functions which satisfy the boundary conditions.

$$P = \sum_{Lm\{m_i',n_i',k_i'\}} a_{Lm}^{m_1'n_1'k_1'\cdots} Y_{Lm}\prod_i \cos\frac{m_i'\pi z_i}{L}\exp(\mathrm{i}n_i'\phi_i)L_{n_i'k_i'}(\omega_{n_i'k_i'}r_i) \tag{5}$$

The Y_{Lm} are spherical harmonics, the m_i' are non-negative integers, and the n_i' are integers. The $L_{n_i'k_i'}$ are linear combinations of Bessel functions of the first and second kind [6] (see Appendix). The coefficients in the linear combination and the partial eigenvalues $\omega_{n_i'k_i'}$ are determined by the boundary conditions. k_i' is a non-negative integer label for the basis functions $L_{n_i'k_i'}$. We seek the time dependence of the expansion coefficients collected according to the power of E. The dynamics of the individual a's is found with the aid of the projection operator

$$\int \mathrm{d}\Omega Y_{Lm}^*\prod_i \int_0^L \frac{(2-\delta_{m_i0})}{L}\cos\frac{m_i\pi z_i}{L}\mathrm{d}z_i \int_0^{2\pi}\frac{1}{2\pi}\exp(-\mathrm{i}n_i\phi_i)\,\mathrm{d}\phi_i \int_{r_1}^{r_2}\frac{1}{A_{n_ik_i}} r_i L_{n_ik_i}(\omega_{n_ik_i}r_i)\,\mathrm{d}r_i \tag{6}$$

The $A_{n_ik_i}$ are normalization factors (see Appendix). $\delta_{m\rho}$ is the Kronecker delta function. The expansion coefficients are collected according to the power of the electric field amplitude

$$a_{Lm}^{m_1'n_1'k_1'\cdots} = {}^0a_{Lm}^{m_1'n_1'k_1'\cdots} + E\,{}^1a_{Lm}^{m_1'n_1'k_2'\cdots} + \cdots \tag{7}$$

Coefficients of E in eq. (1) are collected and the resulting equations solved order by order. The ${}^1a$ coefficients are needed to predict the dielectric relaxation. Only ${}^2a_{20}^{000\cdots}(t)$ is needed to describe the dynamic Kerr effect.

3. The field on response

3.1 Zero order terms

Equation (1) is solved for $E = 0$. The solution is

$$ {}^0P(0) = {}^0P(t) = {}^0P(\infty) = \exp\left(-\frac{V' + V''}{k_B T} \right) \Big/ \int \exp\left(-\frac{(V' + V'')}{k_B T} \right) \mathrm{d}\tau \tag{8} $$

No zero order coefficient changes with time. However, the zero order coefficients are used in the description of the dielectric relaxation and the dynamic Kerr effect, since they are involved in the solution for the ${}^1A$'s and the ${}^2a$'s depend on the ${}^1a$'s. Zero-order expansion coefficients are shown in Section A5 of the Appendix.

3.2 First order terms

$$ \frac{\partial {}^1a_{Lm}^{m_1 n_1 k_1 \cdots}}{\partial t} = -\left[L(L+1)D_\perp + m^2(D_\parallel - D_\perp) + D_3 \sum_{i=1}^{n''} \left(\frac{m_i^2 \pi^2}{L^2} + \omega_{n_i k_i}^2 \right) \right] {}^1a_{Lm}^{m_1 n_1 k_1 \cdots} $$

$$ + \frac{D_\perp}{k_B T} \sum_i \frac{2eL(2 - \delta_{m_1 0})}{\sqrt{3}\pi^2} \sum_{m_i'} - \left\{ \frac{1}{(m_i + m_i')^2} + \frac{1}{(m_i - m_i')^2} \right\} {}^0a_{00}^{m_1 n_1 k_1 \cdots m_i' n_i k_i \cdots} $$

with $L = 1$, $m = 0$ and $m_i + m_i'$ odd

$$ + \frac{D_3}{k_B T} \sum_i \sum_{k \text{ odd}} \frac{4e}{\sqrt{3}L} \left\{ \frac{m_i'}{k} \varepsilon S_{m_i m_i' k} - \varepsilon C_{m_i m_i' k} \right\} {}^0a_{00}^{m_1 n_1 k_1 \cdots m_i' n_i k_i \cdots} $$

with $L = 1$, $m = 0$ and $k = m_i + m_i'$ or $k = m_i - m_i'$ or $k = m_i' - m_i$

$$ + \frac{(D_\parallel + D_\perp)}{k_B T} \sum_i \sum_{k_i'} \frac{ie}{2} \sqrt{\tfrac{2}{3}} I_{n_i 0 n_i - 1 k_i 0 k_i'}^{200} {}^0a_{00}^{m_1 n_1 k_1 \cdots m_i' n_i - 1 k_i' \cdots} $$

with $L = 1$, $m = 1$

$$ + \frac{D_3}{k_B T} \sum_i \sum_{k_i'} \frac{ie}{2} \sqrt{\tfrac{2}{3}} \left\{ n_i I_{n_i 0 n_i - 1 k_i 0 k_i'}^{000} - \sum_k B_{0k} \left(I_{n_i 0 n_i - 1 k_i 0 k_i'}^{111} - \omega_{0k}^2 I_{n_i 0 n_i - 1 k_i 0 k_i'}^{100} \right) \right\} {}^0a_{00}^{m_1 n_1 k_1 \cdots m_i' n_i - 1 k_i' \cdots} $$

with $L = 1$, $m = 1$

$$ + \frac{(D_\parallel + D_\perp)}{k_B T} \sum_i \sum_{k_i'} \frac{ie}{2} \sqrt{\tfrac{2}{3}} I_{n_i 0 n_i + 1 k_i 0 k_i'}^{200} {}^0a_{00}^{m_1 n_1 k_1 \cdots m_i' n_i + 1 k_i' \cdots} $$

with $L = 1$, $m = -1$

$$ + \frac{D_3}{k_B T} \sum_i \sum_{k_i'} \frac{ie}{2} \sqrt{\tfrac{2}{3}} \left\{ -n_i I_{n_i 0 n_i + 1 k_i 0 k_i'}^{000} - \sum_k B_{0k} \left(I_{n_i 0 n_i + 1 k_i 0 k_i'}^{111} - \omega_{0k}^2 I_{n_i 0 n_i + 1 k_i 0 k_i'}^{100} \right) \right\} {}^0a_{00}^{m_1 n_1 k_1 \cdots m_i' n_i + 1 k_i' \cdots} $$

with $L = 1$, $m = -1$

$$+D_3\sum_i \sum_{m_i'k_i'} {}''V^{m_1n_1k_1\cdots m_i'n_i'k_i'\cdots}_{m_1n_1k_1\cdots m_in_ik_i\cdots}\,{}^1a^{m_1n_1k_1\cdots m_i'n_i'k_i'\cdots}_{Lm}$$

$$+D_3\sum_{ij}{}' \sum_{m_i'k_i'm_j'k_j'} {}'V^{m_1n_1k_1\cdots m_i'n_ik_i'm_j'n_jk_j'\cdots}_{m_1n_1k_1\cdots m_in_ik_im_jn_jk_j\cdots}\,{}^1a^{m_1n_1k_1\cdots m_i'n_i-nk_i'm_j'n_j+nk_j'\cdots}_{Lm} \tag{9}$$

The I's and εC and εS are integrals over basis functions, Their definition is found in the Appendix. Expressions for the coupling coefficients $''\mathbf{V}$ and $'\mathbf{V}$ are developed in the Appendix. The n appearing in the last term (in the superscript of ${}^1a_{Lm}$) arises from the dependence of V' on ϕ_i and ϕ_j (see Appendix). Equation (9) is a set of coupled inhomogeneous linear first order differential equations with constant coefficients that can be solved by standard methods [10]. The solution for a chosen collection of ${}^1a$'s (initial condition ${}^1a$'s = 0) is found by the method of variation of parameters [10] that requires as input the matrix of coefficients of the ${}^1a$'s, the eigenvalues of the matrix, and the column vector of inhomogeneous terms (contribution of the ${}^0a$'s). We also solved the system using Runge–Kutta integration to identify the significant terms (because of the running indices m_i, n_i, k_i the kinetic scheme is infinite in extent and must be truncated to find a solution).

3.3 Second order terms—Kerr effect

To describe the dynamic Kerr effect only ${}^2a^{000\cdots}_{20}$ is needed. We have

$$\frac{\partial {}^2a^{000\cdots}_{20}}{\partial t} = -6D_\perp {}^2a^{000\cdots}_{20} - \frac{D_\perp}{k_BT}\sum_{k\,\mathrm{odd}} \frac{4\mathrm{eLn}''}{k^2\pi^2}\sqrt{\tfrac{3}{5}}\,{}^1a^{k00\cdots}_{10}$$

$$+\frac{D_\perp}{k_BT}\sum_{k_i'} \mathrm{i}en''\sqrt{\tfrac{3}{10}}\left\{I^{200}_{00100k_i'}\,{}^1a^{01k_i'\cdots}_{11} + I^{200}_{00-100k_i'}\,{}^1a^{0-1k_i'\cdots}_{1-1}\right\} \tag{10}$$

In the absence of contributions of V' and V'' to the ${}^1a$'s eq. (10) can be written as

$$\frac{\mathrm{d}y}{\mathrm{d}t} + Py = \sum_j B_jA_j\big(1 - \exp(\lambda_j t)\big) \tag{11}$$

with the solution

$$y = \exp(-6D_\perp t)\sum_j B_jA_j\left\{\frac{\exp(6D_\perp t) - 1}{6D_\perp} - \frac{\exp\big[(6D_\perp + \lambda_j)t\big] - 1}{6D_\perp + \lambda_j}\right\} \tag{12}$$

The B_j are found by inspection from eq. (10) and the A_j and λ_j are found by analysis of the first order terms. With coupling from V' and V'' a more complicated expression results (see below).

4. Dielectric relaxation

Although experimental data for monodisperse DNA oligomers are not yet found in the literature, the formalism allows a prediction for the dipolar correlation function γ that (subject to correction for the internal field effect) is related to the complex dielectric permittivity [11]. γ is defined by

$$\gamma = \frac{\langle \mu(0)\cdot\mu(t)\rangle}{\langle \mu(0)\cdot\mu(0)\rangle} \tag{13}$$

γ is related to the field on ${}^1a(t)$'s by [17]

$$1-\gamma=\frac{\sqrt{\frac{4\pi}{3}}\frac{-4eLn''}{\pi^2}\sum_{n\,\mathrm{odd}}{}^1a_{10}^{n00\cdot}(t)\frac{1}{n^2}-\sqrt{\frac{8\pi}{3}}ien''\sum_k{}^1a_{11}^{01k000\cdot}(t)I_{0100k0}^{200}}{\sqrt{\frac{4\pi}{3}}\frac{-4eLn''}{\pi^2}\sum_{n\,\mathrm{odd}}{}^1a_{10}^{n00\cdot}(\infty)\frac{1}{n^2}-\sqrt{\frac{8\pi}{3}}ien''\sum_k{}^1a_{11}^{01k000\cdot}(\infty)I_{0100k0}^{200}} \tag{14}$$

If the terms in ${}''V$ and ${}'V$ were absent in the equations of change for the ${}^1a$'s (as they are for the ${}^1a_{10}$'s in eq. 10), the general form for the evolution of the ${}^1a$'s would be

$$\frac{\mathrm{d}x_k}{\mathrm{d}t}=\lambda_k x_k+C_k \tag{15}$$

with

$$\lambda_k=-\left[L(L+1)D_\perp+m^2(D_\parallel-D_\perp)+D_3\sum_{i=1}^{n''}\left(\frac{m_i^2\pi^2}{L^2}+\omega_{n_ik_i}^2\right)\right] \tag{16}$$

The C_k are found by inspection of eq. (9) and involve the ${}^0a_{00}$'s. The solution of eq. (16) (initial condition $x_k=0$) for the field on case is

$$x_k=\frac{C_k}{\lambda_k}(\exp(\lambda_k t)-1) \tag{17}$$

so

$$\gamma=\frac{\sum_k\left(\frac{C_k}{\lambda_k}\right)^2\exp(\lambda_k t)}{\sum_k\left(\frac{C_k}{\lambda_k}\right)^2} \tag{18}$$

The terms in ${}''V$ and ${}'V$ in eq. (9) cause coupling of the ${}^1a$'s and eq. (15) is generalized to

$$\frac{\mathrm{d}x_k}{\mathrm{d}t}=\sum_j A'_{kj}x_j+C_k \tag{19}$$

The A'_{kj} and C_k are found by inspection of eq. (9). Equation (19) can be solved by the method of variation of parameters [10]. The solution is relatively simple since the A'_{kj} and C_k are independent of time. A formal solution is

$$\boldsymbol{x}(t)=\left[\int_0^\infty\exp[(t-s)\mathbf{A}']\,\mathrm{d}s\right]\boldsymbol{c} \tag{20}$$

where $\boldsymbol{x}$ is a column vector of the x_k, $\boldsymbol{c}$ is a column vector of the C_k and $\exp(t\mathbf{A}')$ is constructed from the eigenvalues (in general complex) of the $\mathbf{A}'$ matrix $\{\lambda'_k\}$ and its elements $\{A'_{kj}\}$ [10]. The (real) solution for a chosen $x_k(t)$ contains a constant term, and terms in $\exp(\mathrm{Re}\ \lambda'_k)$, $\exp(\mathrm{Re}\ \lambda'_k)\sin(\mathrm{Im}\ \lambda'_k t)$, $\exp(\mathrm{Re}\ \lambda'_k)\cos(\mathrm{Im}\ \lambda'_k t)$. Using the parameters found from the analysis of the Kerr effect, we calculated γ from eq. (14). Ignoring the internal field one can then predict the normalized dielectric loss [11].

$$\frac{\varepsilon''}{(\varepsilon_0-\varepsilon_\infty)}=-\int_0^\infty\sin\,\omega t\frac{\mathrm{d}\gamma}{\mathrm{d}t}\mathrm{d}t \tag{21}$$

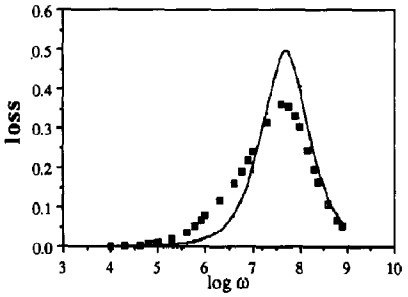

Fig. 1. Normalized dielectric loss as a function of frequency. (□) present model prediction using parameters obtained via regression of dynamic Kerr effect data. (—) Debye model prediction shifted so the frequencies of maximum loss coincide.

The result is shown in Fig. 1. The Debye model result ($\gamma = \exp(-t/\tau)$) is shown for comparison. The simulation of the dielectric loss requires values for the three diffusion constants. We used the values found by regression (uncoupled case) on experimental data of the dynamic Kerr effect (see below). The calculation includes the contribution of coupling and incorporates all modes of appreciable amplitude. The Debye curve is positioned so that the frequencies of maximum loss coincide. The simulated data reflect the contribution of several modes leading to a broad tail at low frequencies and a lowering of the magnitude of the normalized loss at the maximum value.

5. Kerr effect

The ${}^{2}a_{20}^{000\cdots}$ factor is proportional to the transient electric birefringence. Since the constant of proportionality is very uncertain, we normalize to the infinite time response. The relative birefringence is obtained using eq. (12) (no coupling version) as

$$\frac{y}{y(\infty)} = \sum_j X_j \left\{ 1 - \exp(-6D_\perp t) - \frac{6D_\perp}{6D_\perp + \lambda_j} \left[\exp(\lambda_j t) - \exp(-6D_\perp t) \right] \right\} \tag{22}$$

in which j can be considered to be a mode index corresponding to a mode amplitude of

$$X_j = B_j A_j / \sum_j B_j A_j \tag{23}$$

In the presence of coupling (only ${}^{1}a_{1\pm1}$ are coupled) eq. (22) becomes

$$\frac{y}{y(\infty)} = \sum_j X_j' \{ 1 - f_j(t) \} \tag{24}$$

where the X_j' refer to terms having $\exp(\mathrm{Re}\ \lambda_j')$ in f_j. The X_j' are the magnitude of y contributed by a single term divided by the sum of the magnitudes ($t = \infty$).

For a mode to influence the transient birefringence significantly, X_j must be comparable to unity. Data, $y/y(\infty)$(exp), for the field on response taken from ref. [12] are shown in Table 1. Regression to find the parameters $D_\perp$ and D_1 (the surface diffusion constant) gave a sample standard deviation of 0.033 for the normalized birefringence. The backfit, $y/y(\infty)$(condensation), is shown in Table 1. The value of $D_\parallel$ scarcely influenced the fit and was not used as a free parameter. Here we fit the same data varying D_3, $D_\perp$, and $D_\parallel$ (now $D_\parallel$ is an important parameter as a result of freeing motion in the radial direction) and find $D_\perp = 1.398 \times 10^5 \mathrm{s}^{-1}$, $D_\parallel = 6.401 \times 10^5\ \mathrm{s}^{-1}$ and $D_3 = 4.803 \times 10^{-10}\ \mathrm{m}^2\ \mathrm{s}^{-1}$ with a sample

Table 1

Fit to normalized dynamic Kerr effect data for a DNA oligomer

$y/y(\infty)$ (exp)	$y/y(\infty)$ (model)	$y/y(\infty)$ (condensation)	time (μs)
0.006	0.061	0.082	0.246
0.034	0.081	0103	0.293
0.067	0.124	0.145	0.384
0.105	0.127	0.148	0.390
0.132	0.172	0.191	0.480
0.159	0.174	0.193	0.484
0.206	0.223	0.239	0.578
0.250	0.248	0.263	0.627
0.298	0.274	0.286	0.678
0.338	0.321	0.329	0.770
0.379	0.366	0.370	0.862
0.437	0.410	0.411	0.956
0.484	0.469	0.466	1.092
0.545	0.524	0.517	1.230
0.599	0.588	0.577	1.409
0.633	0.618	0.605	1.500
0.670	0.658	0.643	1.634
0.711	0.694	0.678	1.769
0.748	0.735	0.718	1.946
0.785	0.787	0.769	2.208
0.822	0.829	0.811	2.470
0.849	0.867	0.850	2.773
0.872	0.893	0.877	3.032
0.899	0.923	0.909	3.421
0.919	0.944	0.923	3.808
0.935	0.958	0.949	4.151
0.945	0.970	0.961	4.537
0.958	0.979	0.972	4.966
0.971	0.986	0.981	5.438
0.984	0.992	0.989	6.165

standard deviation of 0.026. The backfit is shown as $y/y(\infty)$(model). Several alternative fits are shown in ref. [17].

The calculation was truncated by keeping $k = 1, 3$ in the k sum in eq. (10) and keeping $k_1' = 1, 2, 3$ in the k_1' sum in eq. (10). $'\mathbf{V}$ and $''\mathbf{V}$ do not contribute to the evolution of ${}^1a_{10}^{k00}$ and their effect on ${}^1a_{11}^{01k_1}$ and ${}^1a_{1-1}^{0-1k_1}$ was ignored (at first). Three terms were kept in the expansion of r_i in the basis set. One could keep more terms at the expense of mathematical labor, but little advantage would result as seen by the mode amplitudes X_j listed in Table 2. $j = 1$ and $j = 2$ label the first two "z-modes" ($k = 1$, $k = 3$) and roughly describe the role of the dipole developed by collective motion of the counterions along the direction of the cylinder axis. One sees that only the $k = 1$ mode carries significant amplitude. Similarly $j = 3, 4, 5$ label the first three "ϕ-modes" ($k_1 = 1, 2, 3$) and describe the role of the dipole developed by moving counterions away from the cylinder surface. Again only the first mode contributes significantly to the Kerr effect. Freeing motion in the r-direction allows a previously minor component ($j = 3$) to play a major role. The release of the constraint also improved the quality of fit by reducing the variance by a factor of two. The backfit (shown in Table 1 for the uncoupled case) still shows the systematic deviations (also found previously [1]), especially at short times. The residuals are shown in Fig. 2.

Table 2

Dynamic Kerr effect mode amplitudes and rates

j	No coupling		Coupling	
	X_j	$-\lambda_j\,(s^{-1})$	X_j'	$\lambda_j'\,(s^{-1})$
1	0.570	2.9468×10^6	0.429	2.9468×10^6
2	0.008	2.4284×10^7	0.006	2.4284×10^7
3	0.388	3.3979×10^6	0.538	3.8613×10^6
4	0.044	9.5817×10^6	0.028	$1.35\times10^7-i3.87\times10^6$
5	−0.010	1.9339×10^7	−0.001	$1.35\times10^7+i3.87\times10^6$

Although the quality of fit is improved significantly by removal of the constrant, the model still performs poorly at short times. This observation is not particularly surprising since diffusion is a "long time" proces.

Regression was also performed keeping the coupling terms. The variance decreased by an additional factor of four but unphysical values were found for the diffusion constants ($D_\parallel$ was *negative* at the minimum error point). The mode amplitudes are sensitive to the presence of coupling, but the decay rates of the major modes are not. As we see below, the prediction of the mode amplitudes is questionable.

First we examine the quality of fit as reflected in the data of Table 1 and Fig. 1. Although the quality of fit is improved by allowing radial motion, both the constrained and unconstrained models perform poorly at short times. The actual system response at short times is much slower than predicted by the model calculations. Clearly the onset of the process of developing a dipole to produce the torque that orients the biopolymer is not described by the forced diffusion equation.

Another problem in fitting the data of ref. [12] is that the transient electric birefringence experiment was performed with 1 nM added salt (a necessity to prevent denaturation), whereas the model calculation here is for no added salt. Added salt probably has a large effect on the mode amplitudes.

The experiment yields a negative birefringence indicating dominance of the z-modes over the ϕ-modes. The no salt prediction is just the opposite. A clue to this predicament is found in a (phenomenological) model calculation by Fixman and Jagannathan [18]. This calculation also predicts

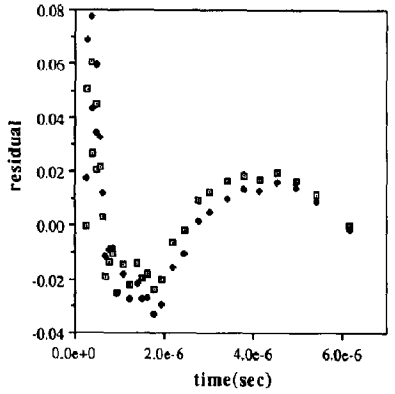

Fig. 2. Residuals ($y/y(\infty)$(model)$-y/y(\infty)$(exp)) from the backfit to dynamic Kerr effect data. (♦)–fit from ref. [1], and (□) present model (uncoupled case).

that, in the absence of added salt, the dominant component of the induced electric dipole moment is perpendicular to the long axis of the cylindrical polyion. Fixman's calculations also predicted that addition of simple electrolyte would decrease the perpendicular component (more so that the parallel component) of the induced moment. At concentrations of about 1 mM (depending on the length of the polyion) the parallel component dominates. Thus a comparison of the model and experimental amplitudes is complicated by the fact that they refer to significantly different conditions. However, the relaxation rates are determined by the diffusion constants $D_{\|}$, $D_{\perp}$ and D_3 which are cleanly defined and the fitting process will force the response to be on the proper time scale even though the predicted shape of the transient electric birefringence exhibits systematic error. In order to obtain a clear comparison, the experiment could be done as a function of excess salt and the zero salt limit taken.

It is appropriate to comment on the magnitude of the model parameters. Regression on the field off data yields $D_{\perp}$, since (field off)

$$y/y(\infty) = \exp(-6D_{\perp}t) \tag{25}$$

Szabo et al. [12] reported 1.28×10^5 s^{-1} by fitting digitized data derivived from Fig. 3 of ref. [12], the Kirkwood–Auer–Riseman equation [14] gives 1.42×10^5 s^{-1}, and the equation of Tirado et al. [15] yield a value of 1.02×10^5 s^{-1} in poorer agreement with the other values. The value of $D_{\perp}$ found here by regression is certainly reasonable. Since $D_{\|}$ did not play much of a role when the calculation involved the surface constraint, we made a wild guess and set $D_{\|} = 10^7$ s^{-1}. Certainly $D_{\|}$ is expected to be much larger than $D_{\perp}$. Regression in the present calculation yields a value of $D_{\|}$ about five times that of $D_{\perp}$. This finding seems acceptable. D_3 can be estimated from the sodium ion mobility in water and we calculate 1.2×10^{-9} m^{2}s^{-1}. The value found here is less than half that. One might be tempted to argue that the sodium ions are moving in a very concentrated electrolyte near the cylinder surface and are thus retarded, but we see that the formalism is supposed to account for the polyion–counterion and counterion–counterion interactions explicitly. The Kerr effect experiments were done in 1 mM added salt so, even accounting for nonuniformity in the added salt concentration, a large reduction in D_3 is not expected. The origin of the discrepancy presumably reflects effects left out of the model picture. For example specific solvent effects are not incorporated. Perhaps diffusion of counterions in the first few hydration layers is slowed by the need to break and make solvent structures.

Appendix. Mathematical details

A1. Explicit expressions for contraction involving the rotation and gradient operators

The contractions in the first and third terms on the right-hand side (r.h.s.) of eq. (1) are most conveniently done in Cartesian co-ordinates and the results subsequently expressed in terms of Euler angles [7] θ and ϕ (the third Euler angle is supressed as the tensor $\mathbf{D}_R$ has spheroidal symmetry). The results are well known and appear regularly in the literature [1].

$$\nabla_u \cdot \mathbf{D}_R \cdot \nabla_u P = D_{\perp} \left\{ \frac{1}{\sin\theta} \frac{\partial}{\partial\theta} \sin\theta \frac{\partial P}{\partial\theta} + \frac{1}{\sin^2\theta} \frac{\partial^2 P}{\partial\phi^2} \right\} + (D_{\|} - D_{\perp}) \frac{\partial^2 P}{\partial\phi^2} \tag{A1}$$

$$\frac{1}{k_B T} \nabla_u \cdot \mathbf{D}_R \cdot P \nabla_u V = \frac{D_{\perp}}{k_B T} \frac{1}{\sin\theta} \frac{\partial}{\partial\theta} P \sin\theta \frac{\partial V}{\partial\theta} + \left\{ \frac{D_{\perp}}{k_B T} \cot^2\theta + \frac{D_{\|}}{k_B T} \right\} \frac{\partial}{\partial\phi} P \frac{\partial V}{\partial\phi} \tag{A2}$$

The second and fourth terms do not involve tensors and are easily evaluated by expressing the gradient operator ∇_i in cylindrical co-ordinates [4]. One finds

$$D_3 \sum_i \nabla_i^2 P = D_3 \left\{ \sum_i \frac{\partial^2 P}{\partial z_i^2} + \sum_i \frac{1}{r_i^2} \frac{\partial^2 P}{\partial \phi_i^2} + \sum_i \left[\frac{1}{r_i} \frac{\partial}{\partial r_i} r_i \frac{\partial P}{\partial r_i} \right] \right\} \tag{A3}$$

$$\frac{D_3}{k_B T} \sum_i \nabla_i \cdot P \nabla_i V = \frac{D_3}{k_B T} \left\{ \sum_i \frac{\partial}{\partial z_i} P \frac{\partial V}{\partial z_i} + \sum_i \frac{1}{r_i^2} \frac{\partial}{\partial \phi_i} P \frac{\partial V}{\partial \phi_i} + \sum_i \left[\frac{1}{r_i} \frac{\partial}{\partial r_i} r_i P \frac{\partial V}{\partial r_i} \right] \right\} \tag{A4}$$

A2. The basis set for the expansion of P

It is natural to choose the eigenfunctions of the free diffusion of operators (terms one and two on the r.h.s. of eq. 1) subject to the chosen boundary conditions. The allowed eigenfunctions of the operator $\nabla_u \cdot \mathbf{D}_R \cdot \nabla_u$ are spherical harmonics and

$$\nabla_u \cdot \mathbf{D}_R \cdot \nabla_u Y_{Lm} = -\{L(L+1)D_\perp + m^2(D_\parallel - D_\perp)\} Y_{Lm} \tag{A5}$$

with $L = 0, 1, 2, \ldots$ and $-L \le m \le L$. The eigenfunctions of ∇_i^2 are separable in the variables $\{z_i, \phi_i, r_i\}$. As shown before [1], the contribution to the eigenfunctions involving z_i and ϕ_i are: $\cos(m_i' \pi z_i / L)$ and $\exp(i n_i' \phi_i)$, where m_i' is a non-negative integer, and n_i' an integer.

The function of r_i involves Bessel functions of order n_i'. The general solution is

$$C_{n_i' k_i'} L_{n_i' k_i'}(\omega_{n_i' k_i'} r_i) = C_{n_i' k_i'} J_{n_i'}(\omega_{n_i' k_i'} r_i) + D_{n_i' k_i'} Y_{n_i'}(\omega_{n_i' k_i'} r_i) \tag{A6}$$

where J and Y are Bessel functions of the first and second kind [6]. The (partial) eigenvalues $\omega_{n_i' k_i'}$ and the ratios of D to C are determined by the two boundary conditions $\partial P / \partial r_i = 0$, $r_i = r_1, r_2$

$$0 = \left(\frac{\mathrm{d} L_{n_i' k_i'}}{\mathrm{d} r_i} \right)_{r = r_1} = \left(\frac{\mathrm{d} L_{n_i' k_i'}}{\mathrm{d} r_i} \right)_{r = r_2} \tag{A7}$$

These two equations are solved (numerically) for the allowed ω's and the corresponding D/C ratios. One finds

$$\frac{D_{nk_i'}}{C_{nk_i'}} = \frac{J_{n+1}(\omega_{nk_i'} r_1) - J_{n-1}(\omega_{nk_i'} r_1)}{-Y_{n+1}(\omega_{nk_i'} r_1) + Y_{n-1}(\omega_{nk_i'} r_1)} = \frac{J_{n+1}(\omega_{nk_i'} r_2) - J_{n-1}(\omega_{nk_i'} r_2)}{-Y_{n+1}(\omega_{nk_i'} r_2) + Y_{n-1}(\omega_{nk_i'} r_2)} \tag{A8}$$

L can be normalized

$$A_{n_i' k_i'} = \int_{r_1}^{r_2} r_i L_{n_i' k_i'}^2(\omega_{n_i' k_i'} r_i) \mathrm{d} r_i \tag{A9}$$

The eigenvalues of the combined eigenfunctions are

$$D_3 \sum_i \nabla_i^2 \prod_i \cos \frac{m_i' \pi z_i}{L} \exp(i n_i' \phi_i) L_{n_i' k_i'}(\omega_{n_i' k_i'} r_i) = \sum_i \left[-\frac{m_i'^2 \pi^2}{L^2} - \omega_{n_i' k_i'}^2 \right] \prod_i (\text{same}) \tag{A10}$$

Table A1 shows some values of ω_{nk} and D_{nk}/C_{nk}.

Table A1

Eigenvalues and coefficients of the Bessel functions

k	ω_{k0}	D_{0k}/C_{0k}	ω_{k1}	D_{1k}/C_{1k}
0	0	0	–	–
1	7.383×10^{7}	7.129×10^{-3}	3.536×10^{7}	-1.663×10^{-3}
2	1.354×10^{8}	2.338×10^{-2}	7.083×10^{7}	-6.694×10^{-3}
3	1.966×10^{8}	4.781×10^{-2}	1.022×10^{8}	-1.399×10^{-2}
4	2.578×10^{8}	7.948×10^{-2}	1.335×10^{8}	-2.387×10^{-2}
5	3.190×10^{8}	1.175×10^{-1}	1.635×10^{8}	-3.577×10^{-2}
6	3.803×10^{8}	1.614×10^{-1}	1.947×10^{8}	-5.062×10^{-2}

A3. Expansion of the potential of interaction of the counterions with fixed charges

Two expressions for V''/k_BT are

$$\frac{V''}{k_BT}=\sum_{i=1}^{n''}\sum_{k=1}^{n''}\frac{-e^2}{4\pi\varepsilon\varepsilon_0k_BT|r_i-r_k|}=\sum_{i=1}^{n''}\sum_{m=0}^{\infty}\sum_{n=-\infty}^{\infty}\sum_{k=0}C_{mnk}\cos\frac{m\pi z_i}{L}\exp(in\phi_i)L_{nk}(\omega_{nk}r_i) \tag{A11}$$

V'' depends on the distribution of fixed charges in the biopolymer as described by the set $\{r_k\}$. Considering short fragments of DNA, two much used models for $\{r_k\}$ (the phosphate charges) are an idealized double helix of point charges (radius 1.0 nm, 3.4 nm per turn) or a discrete (or continuous) line charge on the cylinder axis. One might expect these apparently very different pictures to give radically different results; in fact these two charge distributions look very similar to the counterions. Only terms with $n = 0$ and even m contribute significantly.

To see the role of n in the expansion, consider a fixed value for r_i (1.3 nm say, several values were examined). Using the continuous line charge model, there is *no* dependence of V'' on ϕ_i and so only terms with $n = 0$ contribute. Defining (25°C, $r_1 = 1.3$ nm, $r_2 = 52$ nm, $L = 42.16$ nm)

$$C_m=\sum_{k=0}C_{m0k}L_{0k}(\omega_{0k}r_1) \tag{A12}$$

Values of C_m are shown in Table A2 (note that the C's are inversely proportional to T).

Adopting the idealized double helical distribution of fixed charges, some n-dependence is found and we define

$$C_{mn}=\sum_{k=0}C_{mnk}L_{nk}(\omega_{nk}r_i) \tag{A13}$$

Table A2

Fixed charge expansion coefficients for counterions contrained to a cylindrical surface

m	C_m	C_{m0}	C_{m1}	C_{m2}	C_{m4}
0	-2.734×10^{1}	-2.734×10^{1}	2.799×10^{-8}	1.604×10^{-2}	1.848×10^{-3}
1	-1.189×10^{-5}	-1.187×10^{-5}	0	0	0
2	3.296	3.162	2.543×10^{-8}	1.599×10^{-2}	1.845×10^{-3}
3	-9.936×10^{-6}	-9.975×10^{-6}	0	0	0
4	1.530	1.440	2.450×10^{-8}	1.580×10^{-2}	1.844×10^{-3}
6	9.213×10^{-1}	8.568×10^{-1}	2.371×10^{-8}	1.556×10^{-2}	1.830×10^{-3}

Table A3

Expansion coefficients for V''/k_BT

k	C_{00k}	C_{10k}	C_{20k}	C_{30k}
0	-5.397	-2.298×10^{-6}	3.561×10^{-1}	-2.035×10^{-6}
1	-5.817	-2.555×10^{-6}	9.002×10^{-1}	-1.908×10^{-6}
2	-2.655	-7.336×10^{-7}	5.642×10^{-1}	-8.160×10^{-7}
3	-2.401	-5.145×10^{-7}	4.028×10^{-1}	-8.157×10^{-7}
4	-1.500	-5.090×10^{-7}	2.524×10^{-1}	-5.287×10^{-7}
5	-1.428	-3.683×10^{-7}	1.941×10^{-1}	-5.276×10^{-7}
6	-9.911×10^{-1}	-3.685×10^{-7}	1.311×10^{-1}	-3.767×10^{-7}

Values of C_{mn} (for $r_i = 1.3$ nm) are shown in Table A2. Clearly only even values of m or n are needed and the $n = 0$ terms dominate (the same picture emerges for other choices of r_i). Since C_m and C_{m0} are close in value, the line and helical distributions of fixed charges are virtually equivalent for describing V''.

Some values of C_{m0k} are shown in Table A3. These are computed using the discrete line charge model. An expression for C_{m0k} is found by taking the expansion of $1/|\boldsymbol{r}_i - \boldsymbol{r}_k|$ from the literature [6] and applying the projection operator to the second and third terms of eq. (A11). The result is

$$C_{m0k} = \sum_{k'=1}^{n'} \frac{-e^2}{2\pi^2\varepsilon\varepsilon_0 k_B T}\int_0^\infty d\omega \frac{\omega}{\left[\left(\frac{m\pi}{L}\right)^2 - \omega^2\right]}$$
$$\times\left\{(-1)^{m+1}\sin\omega L\cos\omega z_{k'} - \sin\omega z_{k'} + (-1)^m\cos\omega L\sin\omega z_{k'}\right\}$$
$$\times\int_{r_1}^{r_2} rL_{0k}(\omega_{0k}r)K_0(\omega r)\,dr \qquad \text{(A14)}$$

The $\{z_{k'}\}$ are the positions of the n'' negative charges on the cylinder axis.

Terms with odd m are insignificant and $m = 0$ dominates the m-dependence. *However*, many values of k are needed to describe V''. Convergence as more terms in k are kept can be seen by calculating partial sums over k in eq. (A13). Keeping terms up to $k = 21$ in the sum for C_{m0} yields a partial sum of -24.43 to be compared with the complete sum value of -27.34. If the partial sums are plotted versus $1/k$ a (quadratic) extrapolation to $1/k = 0$ yields -27.23. Clearly a large number of basis functions involving r_i must be kept in the calculation.

A4. Expansion of the potential of interaction of the counterions

Several expressions for $V'k_BT$ are

$$\frac{V'}{k_BT} = \sum_{ij}{}' \frac{e^2}{4\pi\varepsilon\varepsilon_0 k_B T|\boldsymbol{r}_i - \boldsymbol{r}_j|}$$
$$= \sum_{ij}{}' \sum_{m=0}^{\infty}\sum_{n=-\infty}^{\infty}\sum_{k_1}\sum_{k_2} R_{mnk_1k_2}\cos\frac{m\pi z_i}{L}\cos\frac{m\pi z_j}{L}\exp(in(\phi_i-\phi_j))L_{nk_1}(\omega_{nk_1}r_i)L_{nk_2}(\omega_{nk_2}r_j)$$
$$\times\sum_{ij}{}' \frac{e^2}{2\pi^2\varepsilon\varepsilon_0 k_B T}\sum_{n=-\infty}^{\infty}\int_0^\infty dk\,\cos(k(z_i-z_j))\exp(in(\phi_i-\phi_j))I_n(kr<)K_n(kr>)$$

Table A4

Expansion coefficients for V'/k_BT for $m = 0$, 1 and 2 (table is symmetric in the indices k_1 and k_2)

k_1/k_2	0	1	2	3	4
$m = 0$					
0	0.00914	0.01387	−0.00363	0.00284	−0.00137
1	–	0.00926	0.02328	−0.00494	0.00586
2	–	–	0.00623	0.02402	−0.00295
3	–	–	–	0.00404	0.02571
4	–	–	–	–	0.00466
	0	1	2	3	4
$m = 1$					
0	0.00253	0.00331	−0.00084	0.00112	−0.00048
1	–	0.00833	0.00874	−0.00070	0.00277
2	–	–	0.00802	0.01076	−0.00043
3	–	–	–	0.00700	0.01184
4	–	–	–	–	0.00586
	0	1	2	3	4
$m = 2$					
0	0.00094	0.00087	−0.00033	0.00050	−0.00022
1	–	0.00440	0.00317	−0.00032	0.00137
2	–	–	0.00544	0.00466	−0.00018
3	–	–	–	0.00536	0.00570
4	–	–	–	–	0.00508

The expansion of $1/|r_i - r_j|$ in the variables $\{z_i, \phi_i, r_i, z_j, \phi_j, r_j\}$ appears in the literature [6] and leads to the last term in eq. (A15). The projection involving $\{\phi_i, \phi_j\}$ is trivial and complete projection yields

$$R_{mnk_1k_2} = \frac{e^2(2-\delta_{m0})^2}{L^2\pi^2\varepsilon\varepsilon_0 k_B T}\int_0^\infty \mathrm{d}k \frac{k^2}{\left[k^2-(m\pi/L)^2\right]^2}\left[1-(-1)^m\cos kL\right]\int_{r_1}^{r_2}\mathrm{d}r_i\frac{r_i}{A_{nk_1}}\int_{r_1}^{r_2}\mathrm{d}r_j\frac{r_j}{A_{nk_2}}$$

$$\times L_{nk_1}(\omega_{nk_1}r_i)L_{nk_2}(\omega_{nk_2}r_j)I_n(kr<)K_n(kr>) \qquad \text{(A16)}$$

Equation (A16) is a tedious straightforward three-dimensional numerical integral. I_n and K_n are modified Bessel functions of the first and second kind, respectively [6]. Some $R_{m_0k_1k_2}$ values are shown in Table A4.

In contrast with V'' terms with $n \neq 0$ must be kept as well. Excepting $m = 0$ these terms are about $1/3n$ of the corresponding $n = 0$ R's.

A5. Initial values of the expansion coefficients

To solve eq. (1) we need values for the ${}^k a$'s at $t = 0$. Complete dynamical information results from the computation of $P(t)$ with the imposition of a static electric field of amplitude E at $t = 0$. $P(0)$ is given by

$$P(0) = \exp\left(-\frac{(V''+V')}{k_BT}\right)\Big/\int\exp\left(-\frac{(V''+V')}{k_BT}\right)\mathrm{d}\tau \qquad \text{(A17)}$$

Neither V'' nor V' depend on θ or ϕ and $P(0)$ is not a function of E so ${}^1a(0) = {}^2a(0) = \cdots = 0$ and $L = m = 0$ for all nonvanishing a's. One could attempt to calculate the ${}^0a_{00}^{m_1 n_1 k_1 \cdots}(0)$ by applying the projection operator (eq. 6) to eqs. (5) and (A17). This proved to be computationally inefficient. Rather the fact that V' involves pairwise interactions (V'' singlet interaction) *and* the $\{n_i'\}$ play a minor role in V' and V'' forces the result that terms of the type ${}^0a_{00}^{m_1 0 k_1 m_2 0 k_2 000 \cdots}(0)$ dominate. These can be found from the singlet and pair distribution functions in the z- and r-co-ordinates. To find the $P^{(2)}$ (and $P^{(1)}$) functions, the z, ϕ, r space is divided into cells and the calculated quantities extrapolated to zero cell size (infinite grid in the z, ϕ, r space). A Monte Carlo method employing the Metropolis algorithm [9] was used to generate the system configurations for the n″ counterions on the three-dimensional grid of cells. To make the algorithm more efficient, integer arithmetic was employed. At each step in the Metropolis procedure, the number of particles in each z- or r-cell (singlet) or the number of pairs in a given pair of cells (pair) were enumerated and a running total kept. Then, at the end of the run, the ${}^0a$'s were calculated.

$$\frac{{}^0a_{00}^{m_1 0 k_1 m_2 0 k_2 \cdots}}{{}^0a_{00}^{000000\cdots}} = \frac{\left(\prod_{i=1,2} \frac{A_{00}}{A_{0k_i}}(2-\delta_{m_i 0}) \sum_{z_i} \sum_{r_i} \cos\frac{m_i \pi z_i}{L} r_i L_{0k_i}(\omega_{0k_i} r_i)\right) \cdot P^{(2)}(z_1, z_2) P^{(2)}(r_1, r_2)}{\left(\prod_{i=1,2} \sum_{z_i} \sum_{r_i} r_i\right) \cdot P^{(2)}(z_1, z_2) P^{(2)}(r_1, r_2)} \tag{A18}$$

The factors r_1 and r_2 appear in eq. (A18) because the grid of cells is linear in r and the cell volume is proportional to r. Since the $\{z_i\}$ and $\{r_i\}$ are separable in the basis functions, the m and k indices in the a's behave independently. This means the quartet reduced distribution function $P^{(4)}(z_1, z_2, r_1, r_2)$ factors into the product of two $P^{(2)}$'s. The insensitivity of V'' to whether the fixed charges have a helical or line-axis distribution carries over to the calculation of the ${}^0a_{00}$'s. In fact the ${}^0a_{00}$'s are close in value whether the fixed charges are present or absent ($V'' = 0$ but with the counterions constrained to the surface of the cylinder). The main role of the fixed charges here is to force the counterions to be close to the surface of the cylinder.

There is a considerable "end effect" from V'' on the distribution functions. The singlet-z distribution function, instead of acquiring amplitude at the ends of the cylinder (as a result of counterion repulsions) draws in towards the center leaving the ends with amplitude below the average. This is a consequence of the fact that counterions in the center of the rod see more of the negative charge distribution. Nevertheless, this difference does not manifest itself in the dynamic response to electric fields. A clue to this result is that we found previously [8] that the minimum energy configuration for the counterions constrained to the surface of a cylinder with dimensions corresponding to DNA *in the absence of fixed charges* is a double helix in registry with the (absent) phosphate charges.

Values of some typical ${}^0a_{00}$'s are shown in Table A5 (normalized in the sense of eq. A18).

Table A5

Initial values of some expansion coefficients

${}^0a_{000\cdots}^{0100-10} + {}^0a_{000\cdots}^{0-10010} = 2\langle\cos(\phi_1 - \phi_2)\rangle = -4.44\times10^{-4}$

${}^0a_{000\cdots}^{m_1 00 m_2 00}$	$m_1 =$	0	2	4	6
$m_2 =$	0	1	-7.544×10^{-2}	-6.494×10^{-2}	-5.331×10^{-2}
	$m_1 =$	1	3	5	7
$m_2 =$	1	-5.86×10^{-3}	6.20×10^{-4}	5.76×10^{-4}	5.64×10^{-4}
	3	–	-5.20×10^{-3}	5.86×10^{-4}	5.56×10^{-4}
	5	–	–	-4.40×10^{-3}	4.20×10^{-4}
	7	–	–	–	-4.28×10^{-3}

A6. Coupling coefficients for the first order terms

In the text the role of V'' and V' in affecting the evolution of the ^{l}a's was shown in terms of components of matrices $''\mathbf{V}$ and $'\mathbf{V}$ respectively. The matrix coefficients can be obtained by comparing the definition with the expression that results from using the projection operator.

$$
{}''V^{m_1 n_1 k_1 \cdots m_i' n_i' k_i' \cdots}_{m_1 n_1 k_1 \cdots m_i n_i k_i \cdots} = \sum_m \sum_k C_{m0k} \Bigg\{ \varepsilon C_{m_i m_i' m} \left[I^{120}_{n_i 0 n_i k_i k k_i'} + I^{111}_{n_i 0 n_i k_i k k_i'} + I^{010}_{n_i 0 n_i k_i k k_i'} \right] + \left[-\frac{m^2 \pi^2}{L^2} \varepsilon C_{m_i m_i' m} + \frac{m m_i' \pi^2}{L^2} \varepsilon S_{m_i m_i' m} \right] I^{100}_{n_i 0 n_i k_i k k_i'} \Bigg\} \tag{A19}
$$

$$
{}'V^{m_1 n_1 k_1 \cdots m_i' n_i' k_i' m_j' n_j' k_j' \cdots}_{m_1 n_1 k_1 \cdots m_i n_i k_i m_j n_j k_j \cdots} = \sum_{k_1 k_2} \sum_m \sum_n R_{m n k_1 k_2} \varepsilon C_{m_j m_j' m} I^{100}_{n_j n n_j + n k_j k_2 k_j'} \Bigg\{ \varepsilon C_{m_i m_i' m} \left[-n n_i I^{-100}_{n_i n n_i - n k_i k_1 k_i'} \right] + \varepsilon C_{m_i m_i' m} \left[I^{120}_{n_i n n_i - n k_i k_1 k_i'} + I^{111}_{n_i n n_i - n k_i k_1 k_i'} + I^{010}_{n_i n n_i - n k_i k_1 k_i'} \right] + \left[-\frac{m^2 \pi^2}{L^2} \varepsilon C_{m_i m_i' m} + \frac{m m_i' \pi^2}{L^2} \varepsilon S_{m_i m_i' m} \right] I^{100}_{n_i n n_i - n k_i k_1 k_i'} \Bigg\} \tag{A20}
$$

A7. Integrals over basis functions

Application of the projection operator leads to the following integrals:

$$
\int_0^L \frac{(2 - \delta_{m_i 0})}{L} \sin \frac{m_i' \pi z_i}{L} \sin \frac{m \pi z_i}{L} \cos \frac{m_i \pi z_i}{L} \, \mathrm{d} z_i = \varepsilon S_{m_i m_i' m} \tag{A21}
$$

$$
\int_0^L \frac{(2 - \delta_{m_i 0})}{L} \cos \frac{m_i' \pi z_i}{L} \cos \frac{m \pi z_i}{L} \cos \frac{m_i \pi z_i}{L} \, \mathrm{d} z_i = \varepsilon C_{m_i m_i' m} \tag{A22}
$$

Values of these integrals are shown in Table A6.

We also generate integrals over Bessel functions.

$$
I^{abc}_{n_i n n_i' k_i k k_i'} = \int_{r_1}^{r_2} \frac{r_i^a \mathrm{d} r_i}{A_{n_i k_i}} L_{n_i k_i} \frac{\mathrm{d}^b}{\mathrm{d} r_i^b} L_{nk} \frac{\mathrm{d}^c}{\mathrm{d} r_i^c} L_{n_i' k_i'} \tag{A23}
$$

Table A6

Values of trigonometric integrals

$\varepsilon C_{000} = 1$	$\varepsilon S_{000} = 0$
$\varepsilon C_{0mm} = \frac{1}{2}$	$\varepsilon S_{0mm} = \frac{1}{2}$
$\varepsilon C_{mk,mk,0} = 1$	$\varepsilon S_{ml,mk,0} = 0$
$\varepsilon C_{mk,0,mk} = 1$	$\varepsilon S_{mk,0,mk} = 0$
$\varepsilon C_{m,2m,m} = \frac{1}{2}$	$\varepsilon S_{m,2m,m} = \frac{1}{2}$
$\varepsilon C_{mk,m-mk,m} = \frac{1}{2} \mathrm{m} > \mathrm{m_k}$	$\varepsilon S_{mk,m-mk,m} = \frac{1}{2} \mathrm{m} > \mathrm{m_k}$
$\varepsilon C_{mk,mk-m,m} = \frac{1}{2} \mathrm{m_k} > \mathrm{m}$	$\varepsilon S_{mk,mk-m,m} = -\frac{1}{2} \mathrm{m_k} > \mathrm{m}$
$\varepsilon C_{mk,mk+m,m} = \frac{1}{2}$	$\varepsilon S_{mk,mk+m,m} = \frac{1}{2}$
Other cases = 0	Other cases = 0

Some of the I integrals cane be done analytically; others were done numerically using general formulas to express the derivatives in terms of the L's [16]. The integrals have values of the order $\log I = -8(a - 1 - b - c)$.

References

1 W.E. Sonnen, G.E. Wesenberg and W.E. Vaughan, Biophys. Chem. 32 (1988) 283.
2 P.I. Meyer and W.E. Vaughan, Biophys. Chem. 12 (1980) 329.
3 M.E. Rose, Elementary theory of angular momentum (Wiley, New York, 1957).
4 H. Margenau and G.M. Murphy, The mathematics of physics and chemistry (Van Nostrand, New York, 1956).
5 J.A. Altig, G.E. Wesenberg and W.E. Vaughan, Biophys. Chem. 24 (1986) 221.
6 J.D. Jackson, Classical electrodynamics, (Wiley, New York, 1962).
7 H. Goldstein, Classical mechanics (Addison-Wesley, Reading, MA, 1950).
8 G.E. Wesenberg and W.E. Vaughan, Biophys. Chem. 18 (1983) 381.
9 N. Metropolis, A.W. Rosenbluth, M. Rosenbluth, A.H. Teller and E. Teller, J. Chem. Phys. 21 (1953) 1087.
10 A.L. Rabenstein, Elementary differential equations with linear algebra, 3rd edn. (Academic Press, New York, 1982).
11 W.E. Vaughan, Annu. Rev. Phys. Chem. 30 (1979) 103.
12 A. Szabo, M. Haleem and D. Eden, J. Chem. Phys. 85 (1986) 7472.
13 C.F. Anderson and M.T. Record Jr., Annu. Rev. Biophys. Chem. 19 (1990) 423.
14 F. Eirich, ed., Rheology, vol. 1 (Academic Press, New York, 1956).
15 M.M. Tirado, C.L. Martinez and J.G. de la Torre, J. Chem. Phys. 81 (1984) 2047.
16 P.M. Morse and H. Feshbach, Methods of theoretical physics, part II (McGraw-Hill, New York, 1953).
17 W.E. Sonnen, Ph.D. thesis, University of Wisconsin-Madison (1991).
18 M. Fixman and S. Jagannathan, J. Chem. Phys. 75 (1981) 4048.